



Static superconducting gantry-based proton CT combined with X-ray CT as prior image for FLASH proton therapy

Yu-Qing Yang^{1,2,3,4} · Wen-Cheng Fang^{2,4} · Xiao-Xia Huang⁴ · Jian-Hao Tan⁴ · Cheng Wang⁴ · Chao-Peng Wang⁴ · Zhen-Tang Zhao^{2,3,4}

Received: 9 June 2022 / Revised: 20 November 2022 / Accepted: 22 November 2022 / Published online: 25 January 2023

© The Author(s), under exclusive licence to China Science Publishing & Media Ltd. (Science Press), Shanghai Institute of Applied Physics, the Chinese Academy of Sciences, Chinese Nuclear Society 2023

Abstract

Proton FLASH therapy with an ultra-high dose rate is in urgent need of more accurate treatment plan system (TPS) to promote the development of proton computed tomography (CT) without intrinsic error compared with the transformation from X-ray CT. This paper presents an imaging mode of proton CT based on static superconducting gantry different from the conventional rotational gantry. The beam energy for proton CT is fixed at 350 MeV, which is boosted by a compact proton linac from 230 MeV, and then delivered by the gantry to scan the patient's body for proton imaging. This study demonstrates that the static superconducting gantry-based proton CT is effective in clinical applications. In particular, the imaging mode, which combines the relative stopping power (RSP) map from X-ray CT as prior knowledge, can produce much a higher accuracy RSP map for TPSs and positioning and achieve ultra-fast image for real-time image-guided radiotherapy. This paper presents the conceptual design of a boosting linac, static superconducting gantry and proton CT imaging equipment. The feasibility of energy enhancement is verified by simulation, and results from Geant4 simulations and reconstruction algorithms are presented, including the simulation verification of the advantage of the imaging mode.

Keywords Proton therapy · Proton CT · FLASH treatment · Real-time image-guided radiotherapy

1 Introduction

Proton therapy, benefiting from the property of the Bragg peak, has been very popular for several decades as an accurate radiotherapy comprising approximately 85% of hadron therapy in daily tumor treatment [1]. Moreover, FLASH proton therapy, which is popular in R&D has achieved ultra-high dose rates [2], yet requires more precise positioning and better IGRT. Currently, both proton and photon therapies use traditional X-ray CT to construct TPS. The Hounsfield Unit (HU) in the X-ray CT map are converted to RSP values for proton therapy TPS; however, an intrinsic error of 3–5% is introduced into the TPS during the conversion process [3, 4]. Furthermore, organ movement can lead slight differences in range and position to proton treatment when patients are transferred to the treatment room. To solve these problems, proton CT has been proposed as an effective and advanced imaging method to create a direct RSP map for proton therapy TPS with higher accuracy than that converted from X-ray CT.

This work was supported by the Research collaboration on Thailand new synchrotron light source facility (SPS-II) (No. ANSO-CR-KP-2020-16).

✉ Wen-Cheng Fang
fangwencheng@zjlab.org.cn

✉ Xiao-Xia Huang
huangxiaoxia@zjlab.org.cn

¹ Shanghai Institute of Applied Physics, Chinese Academy of Sciences, Shanghai 201800, China

² University of Chinese Academy of Sciences, Beijing 100049, China

³ School of Physical Science and Technology, ShanghaiTech University, Shanghai 201210, China

⁴ Shanghai Synchrotron Radiation Facility, Shanghai Advanced Research Institute, Chinese Academy of Sciences, Shanghai 201204, China

The concept of proton CT was first proposed in the 1960s [5] and has had continuous R&D for several decades [6–8]. Proton CT can reduce range inaccuracies by directly measuring RSP, which is a very effective technique to improve the performance of proton therapy. Due to the growing concern over the radiation dose delivered to patients, low-dose CT is of great interest. Though it can reduce the X-ray radiation dose, it compromises quality and decreases diagnostic performance [9, 10]. Proton CT was found to have a dose advantage compared to X-ray CT; nevertheless, the results of early experimental projects were not sufficient due to the lack of spatial resolution caused by multiple Coulomb scattering. The expected resolution of proton CT can reach 1 mm; however, the error caused by organ motion may occasionally be higher than that caused by proton CT itself, such as in the abdominal cavity. When using proton imaging, localization of lesion position and treatment can be achieved in the same therapy room; thus, the impact of organ movement can be reduced in TPSs. In order to ensure that the residual dose remaining in the human body is as low as possible, the proton imaging energy range is defined as 300–350 MeV [11]. Currently, there is considerable interest in the development of clinical proton systems, while proton CT is still in the experimental stage. If proton CT is integrated with the existing rotational gantry to irradiate the patient, this process takes a long time and is greatly affected by breathing movement. In view of the design of the superconducting therapy gantry in reference [12], this device provides a good choice for the realization of FLASH therapy. Since the number of coils of the device is limited and the irradiation angles are not enough for accurate image reconstruction, new ideas have been proposed to meet the needs of proton imaging, namely proton CT device can be integrated into the static superconducting therapy gantry. In order to solve the problem of sparse information acquisition angles and accelerate the imaging speed, it is a good choice to consider the combination of X-ray CT and proton CT. Besides, the first domestic proton therapy device built in Ruijin Hospital Proton Therapy Center, Shanghai Jiaotong University School of Medicine, which currently provides the proton beam of 70–235 MeV, has entered the clinical experimental stage. It not only marks the historic breakthrough of the first proton device in China, but also puts forward practical conditions for proton CT research.

This paper presents the conceptual designs of a boosting linac, static superconducting therapy gantry, and proton CT imaging device. The proton beam was boosted from 230 to 350 MeV by a compact proton linac. Proton CT device integrated into the static superconducting gantry can achieve a new imaging mode. In this case, the RSP map converted from the X-ray CT image using the HU to RSP conversion curve can be used for prior knowledge, and then 12-angle proton projections can be used for proton image

reconstruction with algebraic reconstruction technique (ART) algorithm. This not only produces a high-accuracy RSP map for TPSs, but performs ultra-fast imaging processes with practical significance for real-time IGRT. Details on the principles of the imaging mode are introduced in this paper, and the results based on Geant4 simulation are presented.

2 Proton CT principle and layout of conceptual design

The design is based on static superconducting gantry. Protons are accelerated and captured into the therapy room. The proton CT system mainly consists of two parts, as illustrated in Fig. 1a. The proton beam enters from the left. The transverse positions of an individual proton in front of and behind the patient are measured using tracking detectors, and a residual range detector is used to determine the proton energy loss in the patient. Thus, the water-equivalent path length (WEPL) of the proton as it passes through the patient can be calculated using a calibration procedure. It is assumed that the energy of an incoming proton is equal to that of a proton ejected from the accelerator. The information is collected as the basis for reconstructing a volume using the RSP.

When the proton energy in proton CT is sufficiently high to fully traverse the phantom, the mean energy loss dE per unit path length dl is described by the Bethe–Bloch equation [13].

$$-\frac{dE(E, \mathbf{r})}{dl} = SP(E(\mathbf{r}), I(\mathbf{r})), \quad (1)$$

where E is the proton energy, I is the material mean excitation energy at position r , and SP is the stopping power in the reference medium. For proton imaging, the RSP corresponds to the ratio of the local stopping power of the material, SP_m , to the stopping power of water, SP_w .

$$RSP = \frac{SP_m}{SP_w} \quad (2)$$

Thus, it can be written as the integral RSP along the proton trajectory L [14].

$$WEPL = \int_L RSP(\mathbf{r}) dl = - \int_{E_{in}}^{E_{out}} \frac{1}{SP_w(I_w, E)} dE, \quad (3)$$

where $SP_w(I_w, E)$ is the stopping power of water, and I_w is the mean excitation energy of water, E_{in} is the incoming energy of the proton, and E_{out} is the outgoing energy.

However, the scattering of protons in the target is not negligible, which tends to change the direction of charged

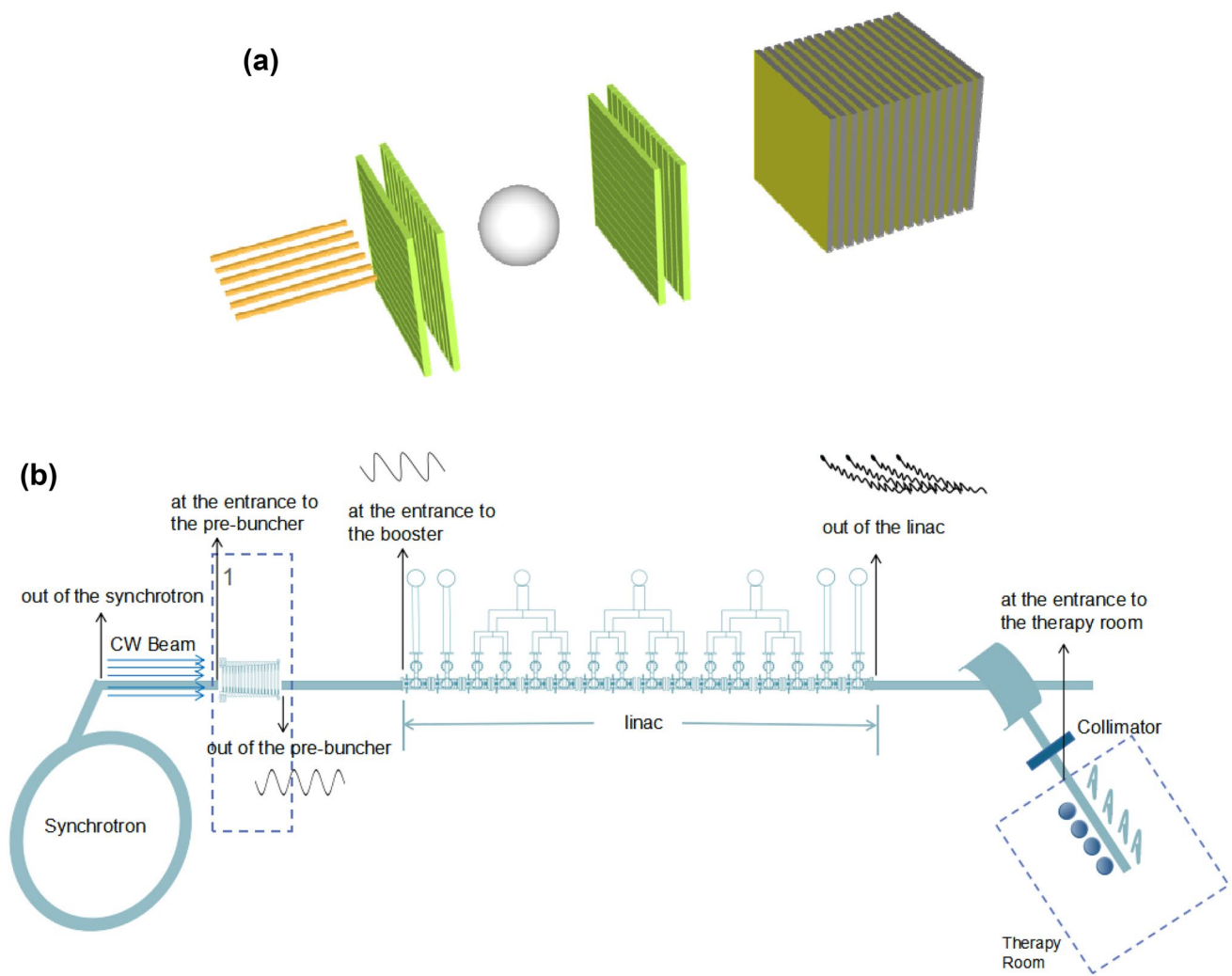


Fig. 1 (Color online) Schematic diagram of 350 MeV proton CT system, including proton scanning principle and the energy enhancement principle. **a** Illustration of the proton CT system. **b** Schematic dia-

gram of energy acceleration from 230 to 350 MeV for the proton CT device. The bunching structure is shown in the dashed square marked 1

particles without changing the total momentum when crossing the phantom [15]. Therefore, to achieve higher resolution, it is necessary to introduce the most likely path in image reconstruction from the detected entry and exit positions and angles [16]. The primary goal of proton CT is to directly construct the 3D distribution of the RSP. Proton CT is expected to achieve a spatial resolution of less than 1 mm and a density resolution of 1% [17]. When integrated into the FLASH device, it is expected to be much faster.

Based on S-band high-gradient technology, beam distribution systems, static superconducting gantry, ultra-fast proton scanning, and proton detection and imaging technology, the energy of protons can be increased from 230 to 350 MeV. The protons are boosted by the accelerating structure and then transmitted to the treatment room, where proton therapy and proton CT devices are installed. The S-band high-gradient accelerating structure meets the

requirements of small, compact facilities and can be used in single treatment rooms as well as in FLASH proton therapy. A similar structure used to accelerate protons was previously demonstrated, and the structure has been cold-tested and the result shows that the design is feasible [18, 19]. The prototype is consistent with the design in this study. The S-band high-gradient accelerating structure can directly accelerate the proton beam generated by a linear accelerator. However, for the proton beam generated by synchrotron and cyclotron, a bunching structure is required to induce micro-bunching of the proton beam before linear acceleration. Figure 1b shows the schematic diagram of accelerating the proton beam generated by the synchrotron. Pre-buncher makes energy modulation only several μ s by picking up from continuous wave (CW) beam, and then makes density modulation. Most particles are bunched together before entering the linac. After the

bending magnet and collimator, bunched proton beam can be transferred to the therapy room for proton imaging.

3 Energy booster design by S-band high-gradient proton linac

In order to verify the feasibility of this design, simulations were carried out. The magnet layout diagram is shown in Fig. 2a. There are 16 accelerator tubes in total and the energy gain of each tube is 8 MeV. As shown in Fig. 2b, the step-up section represents the energy enhancement of the proton through accelerator tubes. It should be noted that proton energy has been increased to 350 MeV with only 15 accelerator tubes in our simulation. But in reality, to prevent the influence of other factors, 16 acceleration tubes are proposed. The extra accelerator tube is a spare. The X – Y phase space diagram of CW beam produced by synchrotron is shown in Fig. 2c. By simulating the distribution of the entire continuous beam group over a period, it was found that the total energy passing rate was 81.2% under ideal conditions. Thus most particles are boosted and transferred through the linac. However, longer tails exist at lower proton energies, and the desired protons are captured. It was calculated that the capture rate is about 45.4% for particles with the energy of 350 ± 1 MeV. Meanwhile, a high-gradient radio-frequency (RF) gun operated in CW mode is required in various accelerating applications for further improve the performance of accelerators [20, 21]. Due to the relatively low beam intensity requirements of proton CT, which equal to 10% of the treatment intensity, the beam loss can still meet the requirements of radiation protection and the capture rate of proton can also be optimized further. According to the simulation results, it is feasible to enhance the proton beam energy from 230 to 350 MeV based on proton linac S-band high-gradient technology.

4 Static superconducting gantry-based proton CT with X-ray CT for prior imaging

At present, proton CT integrated into a conventional rotational gantry is under consideration, although it is still in the experimental stage. While the traditional gantry weighs much heavier and relies on mechanical movement, and the energy changes are determined by a switching magnet. In the rotating process, the patient's breath-holding time is long; hence, the influence of organ movement cannot be ignored. In addition, in proton therapy, improper quantification of safety margins may have more severe consequences than in photon therapy. Margins underestimating may cause part of the target receiving no dose because of a potential shift of the sharp distal

dose falloff. It is also harmful to sensitive organs [22]. These factors restrict the realization of real-time IGRT in proton CT, though it may be a viable option to enable direct and precise localization of lateral tumor. Therefore, a new generation of gantry is needed to meet the requirements of proton therapy.

The new proton CT device consists of the following components: a booster, fast kicker, static superconducting gantry, fast proton beam scanner, and proton imaging system, which can replace the magnet rotation and realize fast scanning of the proton beam with different angles. The fast beam kicker and scanner are realized using an advanced deflector with variable polarization [23], refer to the deflector operating at two modes proposed in 2015 for measurement of beam slice features in both X – Y directions. Owing to the variable polarization RF deflector between the linac and the gantry, the integration of proton imaging and therapy can be achieved without any magnetic field changes or mechanical movement. Compared with the FFAG gantry, they are the same in the design of irradiation without rotation of the magnet [24].

The new static superconducting gantry consisting of several identical superconducting coils is lightweight and capable of delivering proton beams of different energies for proton imaging and therapy. A schematic of a single coil is shown in Fig. 3a. The different colored lines represent proton beams of different energies. They are finally delivered to the same iso-center position of the patient after deflection. In order to accelerate the acquisition speed of proton CT, it is considered to reduce the number of scanning angles of the gantry, similar to a previously constructed device [12]. The difference is that the gantry proposed in this paper consists of several static superconducting coils in 24 directions instead of 12, each with the ability to direct the energy of proton beams up to 350 MeV. However, because the parallel beam has the symmetry property for imaging, and 12 of the coils are distributed in the opposite direction of symmetry to the other 12 coils, only 12 coils are needed for proton imaging within 180° . While 12 coils in Ref 24 can provide projection information from 6 angles of parallel beam, it may not provide enough projections of angles for proton CT.

After a S-band high-gradient accelerating structure, the proton beam passes through a set of ultra-fast proton beam distribution system. The proton beam can be deflected under the action of transverse deflection to realize the solid angle distribution. The proton beam is able to be guided to the downstream superconducting coil unit from different angles by the ultra-fast low-level technology. Different proton beams can be uniformly and orderly emitted to different transverse positions of the imaging object over time, through different solid angles. Because of the energy for imaging is constant, an ultra-fast bunch kicker is needed to deflect the beams into the coils at different angles without

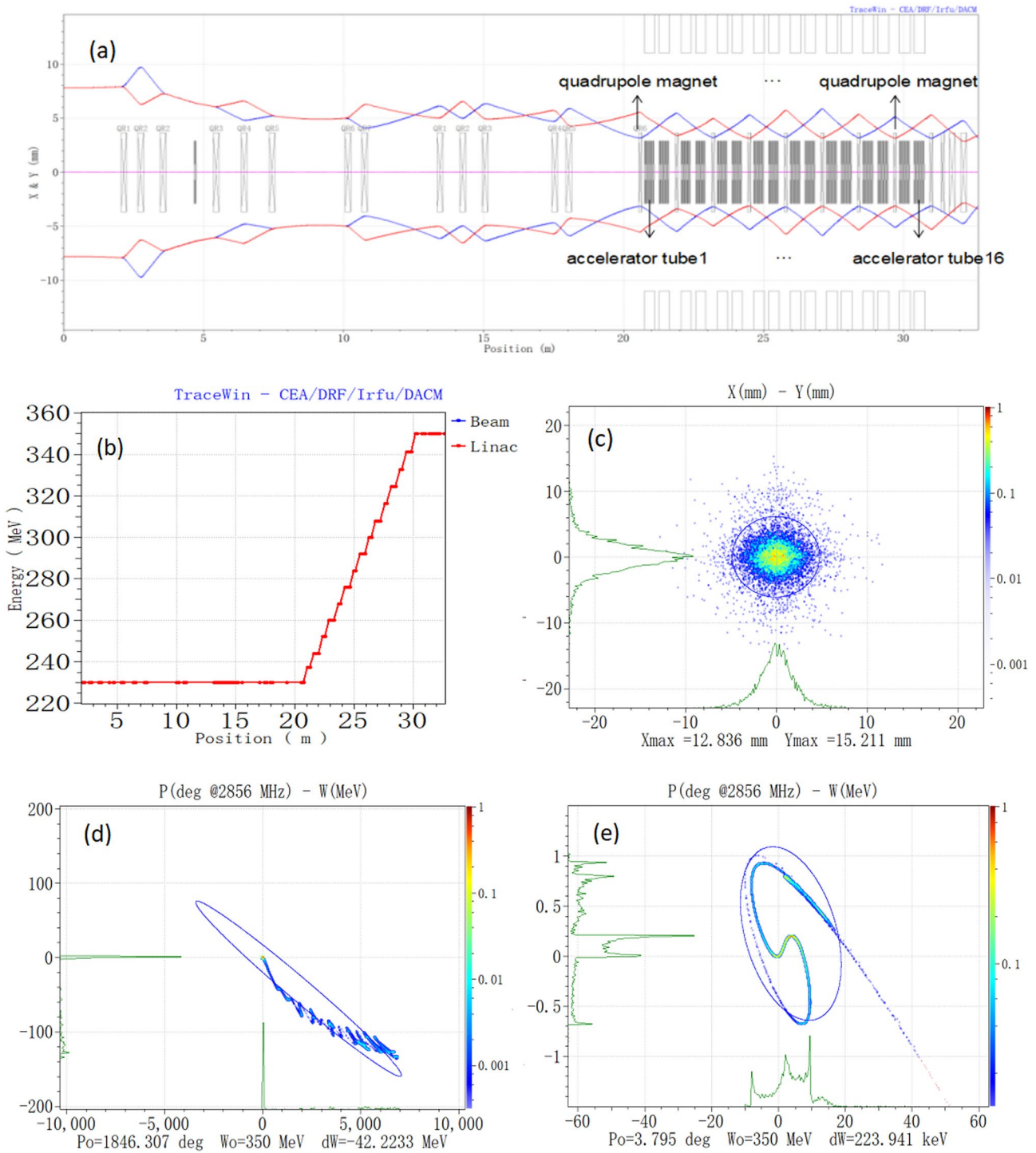


Fig. 2 (Color online) Simulation results of the design for increasing proton energy from 230 to 350 MeV for proton CT. **a** The magnet layout diagram of the energy acceleration structure. **b** Energy acceleration simulation diagram. The abscissa is the beam direction position and the ordinate is the beam energy. **c** The X–Y phase space diagram

of proton beam generated by synchrotron in the form of CW mode. **d** The total energy passing rate is close to 81.2% under ideal conditions over a period. **e** For protons with the energy of 350 ± 1 MeV, the capture rate is about 45.4%

magnet changes. Rapid energy conversion ensures that after proton CT is completed, energy can be quickly switched to the energy range required in proton therapy.

One of the advantages of the static superconducting gantry is that it avoids the influence of mechanical movement. A conceptual design of the gantry is shown in Fig. 3b. Ideally,

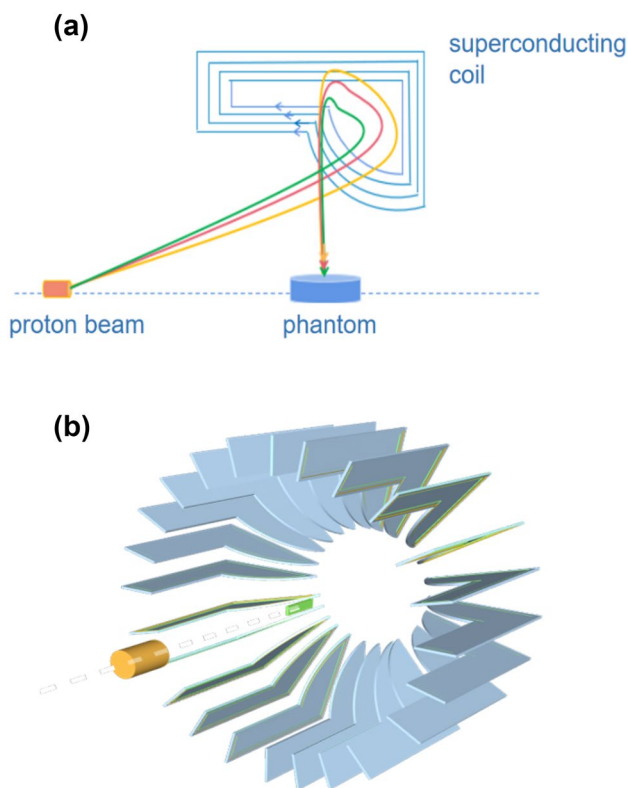


Fig. 3 (Color online) Schematic diagram of the static superconducting gantry. **a** A schematic diagram of a single superconducting coil. **b** Static superconducting gantry proposed to realize 12-angle imaging mode of parallel proton beam. The proton beam enters the therapy system from the left

each coil connects a proton CT device. Only where the coil is can the proton beam pass through. The position detectors are distributed around the human body inside of the gantry, and the residual energy detectors of proton CT are installed outside of the gantry to detect the residual proton energy and absorb the remaining protons. Based on this kind of gantry, the proton bunch rotates around the human body and the gantry does not, which is an important factor in achieving rapid proton irradiation. However, considering 12 angles for sparse imaging, an imaging mode that combines proton CT with X-ray CT is proposed. Before proton irradiation, the patient must take photon irradiation to get a X-ray CT image of the same part of the body. Then, the HU units need to be converted to RSP using the HU to RSP conversion curve. Typically, this curve requires measurement of the HU and RSP of different materials on clinically used X-ray CT and proton therapy equipment to obtain the relationship. The transformed image will simply be referred to as HU-RSP image in the following of this paper. And then the HU-RSP image will be used as prior knowledge for proton image reconstruction in proton therapy. In the proton therapy room, the patient is irradiated with proton beam at 12 different

fixed angles within 180° . The 12-angle projections can calibrate the RSP value of the prior image. It is known that fast scanning systems take approximately $10 \mu\text{s}$ to scan an energy layer [12]. Assuming that there are 1000 points in the scanning layer corresponding to each angle and the scanning area is set as $30 \times 30 \text{ cm}^2$, the acquisition process is able to be completed within 1 ms. This can greatly reduce a patient's breath-holding time in clinical settings. For some sensitive organs and tissues, even a slight movement can have a significant impact on treatment; hence, this technique will reduce the current shortcomings of the procedure. After imaging, the gantry can quickly transform energy required to perform proton therapy, which has a strong clinical significance to realize real-time IGRT.

This proposed imaging mode is based on a novel static superconducting gantry, and the effects of breathing movement and the lateral range error caused by the conversion from HU to RSP can be resolved. Thus, the accuracy of TPSs can be improved. Although the imaging mode based on the static superconducting gantry can improve the acquisition speed of human body, it also puts forward higher requirements on hardware, such as the response speed of graphics processing unit. However, the technique's biggest drawback is its higher cost compared with X-ray CT. While it is worth studying that this approach is predictably capable of real-time IGRT for proton therapy in both the transverse and longitudinal directions.

5 Demonstration of the proton CT image mode by Geant4 simulation

In the previous sections, the proton CT imaging mode based on static superconducting gantry was introduced. Several simulation results are illustrated to compare and verify the different proposals of this study. The software platform for proton CT simulation consists of modules for Geant4 simulation, WEPL calibration, and image reconstruction. The beam is proton parallel beam. The simulation process and results are shown below.

As simulated, the equivalent depth in water of Bragg peak corresponding to 350 MeV proton beam is about 653.5 mm. Thus, it is more efficient in protecting human organs because of less radiation compared to 230 MeV proton CT, which is important for the clinical applications of proton CT. An important step in proton imaging involves calibrating the proton CT simulation platform to obtain the relationship between the WEPL and residual energy or the range. That is, it is necessary to determine the amount of energy lost for each step in the phantom. In this study, a spherical calibration phantom of polystyrene with an RSP of 1.038 was used in Geant4 simulation. The diameter of the phantom lies in the same plane as the center of the proton beam. The flat

beam width must be slightly larger than the diameter of the phantom to make sure that the proton path length covers the phantom. The plane was a regular circle; thus, different diameters can be approximated as different proton paths. Therefore, the residual energy along different path lengths in the phantom was recorded to obtain this calibration relationship curve. Guided by the form of the Bethe-Bloch equation, the stopping responses were fitted with a second-order polynomial function $WEPL = p_0 + p_1E + p_2E^2$, where p_0 , p_1 , and p_2 are fit parameters, and E is the calorimeter response [25]. The resulting calibration function is shown in Fig. 4. The red dots represent particle trajectories in Geant4 simulation, and the blue curve is the fitting relationship curve of WEPL and E . WEPL is represented by R in Fig. 4.

Image reconstruction is a very important part of proton CT. There are two image reconstruction methods using proton CT data: filtered back projection (FBP) and the ART algorithm. FBP filters the acquired projection function and back projects the modified projection data to obtain the value of each pixel. The ART belongs to a class of iterative algorithms; hence, it can be used to solve a linear system in the form of the equation [26]:

$$Ax = b. \tag{4}$$

In proton CT applications, x is the unknown N -dimensional image vector RSP, and b is the M -dimensional vector, which represents the projection value of the proton beam. The system matrix A is a $M \times N$ matrix whose elements a_{ij} represents the contribution of the i th projection to the j th pixel. The calculation of the weight factors a_{ij} directly affects the speed and precision of the reconstruction.

ART is the preferred way of accommodating scattered proton paths. Although the reconstruction speed of FBP is fast, it has a higher requirement for the completeness of

reconstructed data, that is, high resolution image reconstruction cannot be achieved if there are few scanning angles. While ART algorithm is able to achieve sparse angle imaging, and the imaging mode in this paper is more appropriate for ART. Considering the impact of multiple Coulomb scattering, incorporating the factor of most likely path may improve the reconstructed resolution compared with straight line path of protons. The calculation of projection matrix is a key factor in ART algorithm. Only an accurate projection matrix can be generated to reconstruct high-quality images, which also affects the reconstruction speed. Moreover, different algorithms require a unified standard to test their performance and hence judge the reconstructed image quality. The normalized root mean square error d was used as the criterion in this study [27, 28].

$$d = \left[\frac{\sum_{u=1}^N \sum_{v=1}^N (t_{u,v} - r_{u,v})^2}{\sum_{u=1}^N \sum_{v=1}^N (t_{u,v} - t_{mean})^2} \right]^{1/2}, \tag{5}$$

where $t_{u,v}$ and $r_{u,v}$ represent the pixel densities of row u and column v in the original image and reconstructed image of the phantom, respectively, and t_{mean} represents the average pixel density of the phantom. The image has $N \times N$ pixels. Therefore, the smaller the d value, the smaller the deviation from the original image.

5.1 Comparisons of angle numbers and reconstruction methods

To reconstruct the image, a sphere of water with a diameter of 15 cm was used in Geant4 simulation, in which two spheres of different sizes and materials were set. The smallest radius of the sphere is 3 cm of air material, and the other one is a 5 cm diameter sphere made of Teflon material. For each rotational angle, the residual energy and the position of each proton inlet and outlet of the phantom were recorded. Besides, the proton beam was set to be parallel beam of 350 MeV. And the number of protons in each direction is 200,000. Before reconstruction, a screening of proton paths was needed to select protons whose paths are likely to be straight [29]. Then, the data obtained were arranged in the form of a matrix to generate the reconstructed images. Considering the symmetry of the parallel proton beam, the numbers of scanning angles were set to 30°, 60°, 90°, 150° and 180° within 180°, respectively. The results of image reconstruction are shown in Fig. 5a. The gray value of the grayscale image represents the reconstructed RSP.

Through comparison, it was found that the reconstruction results of the ART algorithm were better than those of FBP when there were fewer angles of projections. The calculation results for d are shown in Fig. 5b. The overall d result of ART is horizontally smaller. If the

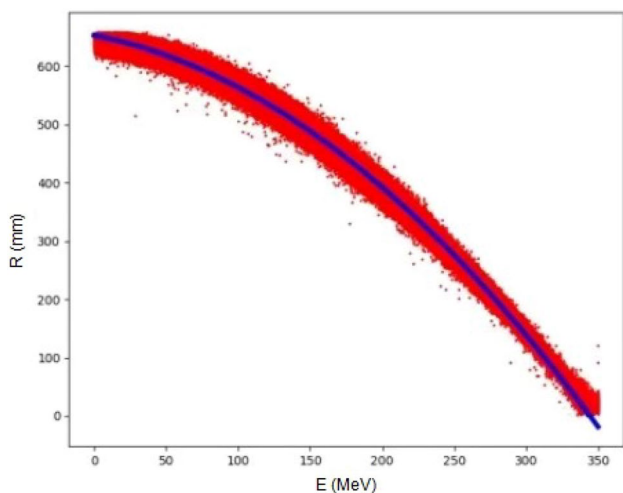


Fig. 4 (Color online) The simulation of the WEPL calibration of 350 MeV proton CT

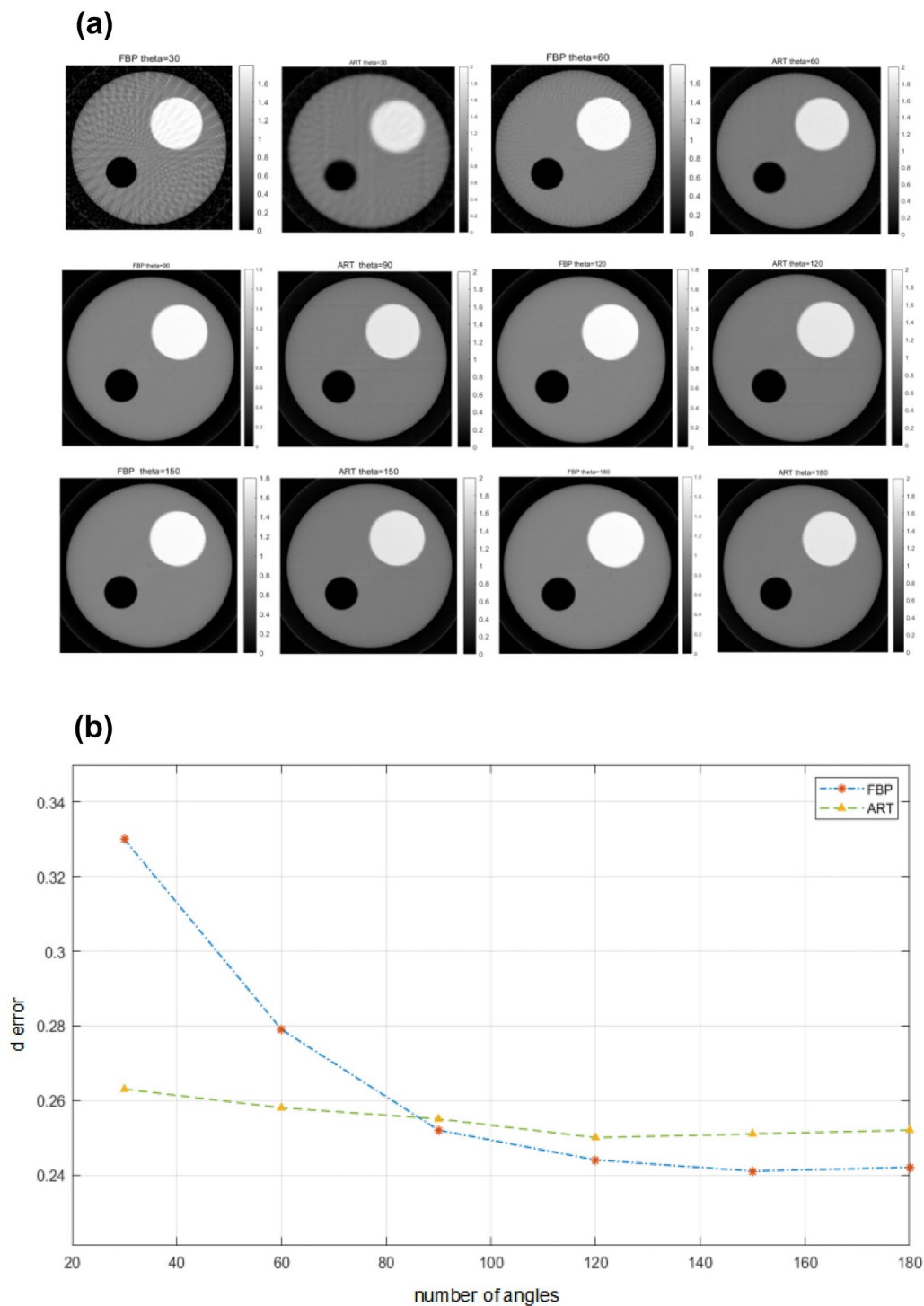


Fig. 5 Results of the comparisons of angle numbers and reconstruction methods. **a** Reconstructed results with FBP and ART, and the number of scanning angles are 30, 60, 90, 150 and 180, respectively, within 180°. The X–Y coordinate represents the position, and the gray

value represents the RSP value. **b** The comparison curve results of the two reconstruction methods. The blue curve represents the result of d value using the FBP method and the green curve represents the result of the ART method

number of angles is sufficient, the results of ART and FBP are similar. It is possible that the result of FBP is better than that of ART when most likely path is not

considered. However, in the case of a small number of scanning angles, the reconstruction results of ART are clearly better. When the number of projection angles

was greater than 90, the reconstructed d value reached a basic saturation trend. Therefore, 60 projection angles are enough for image reconstruction with a suitable algorithm. Compared with the case of collecting information every 1°, the scanning time is reduced. The predicted and reconstructed RSP values of the 60 angles are listed in Table 1. The reconstructed RSP value is close to the predicted value based on the results. The factor of most likely path will be integrated to the ART algorithm so as to improve the resolution of proton imaging in further study.

Table 1 Results of reconstructed RSP of Geant4 simulation with 60-angle projections for ART reconstruction

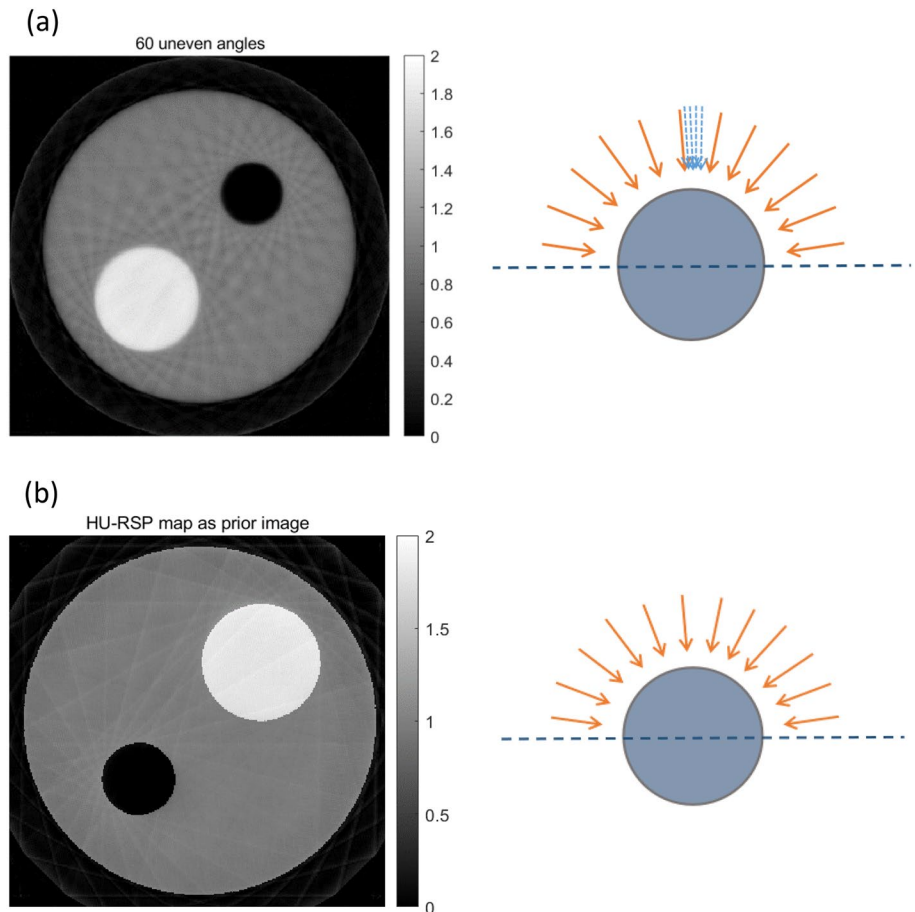
Corresponding serial number	Material	Predicted RSP value	Reconstructed RSP value
1	Teflon	1.78	1.798
2	Air	0.004	0
3	Water	1.00	0.98

5.2 Simulation results of the imaging mode based on static superconducting gantry

The benefit of the imaging mode based on static superconducting gantry is validated in this section. In the simulation, in order to accelerate the imaging speed of proton CT, multiple groups of uneven angles were set for imaging. For example, 12 angles were taken within the range of 180°, and each coil is 15° apart. Each coil can rotate 4 small angles of 2° each time. In other words, each coil can rotate 5 times at 2° intervals of small angles. This imaging mode is compared with the simulation results of the imaging mode based on X-ray CT as prior image proposed in this paper in Fig. 6. As shown in Fig. 6a, the initial iteration matrix was a zero matrix in simulation. The imaging mode with uneven angle reconstruction is feasible, but there are artifacts in the image. This is because although the number of projections is enough, the angles are sparsely distributed. Therefore, sparse angle iterative reconstruction is considered to improve the image quality later.

In the process of verifying the imaging mode proposed based on static superconducting gantry, the value of the standard RSP image is scrambled to pretend to be a HU-RSP image for iteration in the simulation. This image was used as

Fig. 6 Simulation results of the imaging modes. **a** Left: The Geant4 preliminary verification result of Mode1. Right: A schematic diagram of the projection mode. The dashed line indicates the rotational coil position, and each coil has the same four other angles of rotation. **b** Left: The Geant4 preliminary verification result of Mode2. Right: A schematic diagram of the projection mode



a prior image, and then 12-angle proton irradiation was used for calibration within 180° . From the reconstructed result shown in Fig. 6b, this imaging mode was able to achieve a clear image. The pixel value of the image was close to the predicted value. Artifacts in the image will be improved and further optimization of this imaging mode was conducted.

The d values of the two imaging modes were calculated. For clear comparison, Mode 1 is set as the imaging mode of 60 uneven angles, and Mode 2 is set as the imaging mode based on prior image. As shown in Table 2, the values of d_{\min} for Mode 1, Mode 2 are 0.253, and 0.09, respectively, and the values of $d_{\text{iter}10}$ are 0.255, and 0.15, respectively. It should be noted that d_{\min} represents the value with the smallest value of d in 10 iterations, and $d_{\text{iter}10}$ represents the d value of the image after 10 iterations. Based on the reconstructed data, Mode 1 and Mode 2 are feasible. And Mode 2, which combines the HU-RSP image as prior knowledge, has the lowest d value. This is because the HU-RSP image provides a good initial image for the image iteration, and then 12-angle proton projections can modify and calibrate the RSP value. The error caused by the conversion of HU to RSP can be corrected by the actual irradiation of protons. In addition, Mode2 was found to take the least amount of time during reconstruction. However, because the calculation of the projection matrix in the algorithm were not

processed rapidly in this study, the time data are not listed. Through comparison, the Mode 2 method, which represents the imaging mode based on static superconducting gantry, can improve the image quality.

5.3 Summary of requirements for proton CT based on static superconducting gantry

It is proved that it is feasible to realize proton energy enhancement based on S-band high-gradient accelerating structure to perform proton CT based on static superconducting gantry in the treatment room, through preliminary simulation. And the imaging mode based on X-ray CT as a prior image shows relatively superior advantages. In order to promote the engineering realization of proton CT, the index requirements are summarized, according to the results and conditions in the simulation. The parameter requirements are shown in Table 3.

6 Conclusion

This paper introduced the conceptual design of a 350 MeV proton CT system composed of a linac, static superconducting gantry, and proton CT imaging equipment, which can be applied and integrated to different accelerators for FLASH proton therapy. And the imaging mode of proton CT is proposed based on static superconducting gantry. Results from Geant4 simulations indicate that the proton imaging mode based on X-ray CT image as prior image is a practical and effective method to produce high-precision images. With ultra-fast image time, proton CT can be used

Table 2 Comparisons between the calculation results of d_{\min} and d_{10} of the two imaging modes. The number of setting angles for Mode1 is 60, and the number for Mode2 is 12

Mode	d_{\min}	d_{10}
Mode1	0.253	0.255
Mode2	0.09	0.15

Table 3 Summary of parameter requirements for proton CT based on superconducting therapy gantry

	Parameter	Target value	
Gantry	Type	Static superconducting gantry	
Proton beam	Beam energy	350 MeV	
	Energy spread	0.1%	
	Events of one profile		10^8 (90 angles)
			10^7 (12 angles)
	Events of one spot	10^3 – 10^4	
Dose		Human body: < 3.25 cGy	
		Head: ~ 1.2 cGy	
Position detector	Resolution	< 0.5 mm	
	Readout rate	~ 100 kHz	
Energy detector	Energy resolution	0.3–0.6%	
	Decay time	~ ns	
Time	Scanning time of one angle	~ ms	
	Total scanning time	~ s	
Image quality	Spatial resolution	1 mm (Radiation Field of $10 \times 10 \text{ cm}^2$)	
		2 mm (Radiation Field of $30 \times 30 \text{ cm}^2$)	
	RSP accuracy	~ 1%	

as a breakthrough technique for FLASH proton treatment. In order to develop proton CT for clinical applications, further simulations on this imaging mode proposed are necessary. In this respect, a project has been approved to build a proton CT prototype to verify the principle and the imaging mode of proton CT proposed in this paper.

Author contributions All authors contributed to the study conception and design. Model design, simulation calculation and analysis were performed by Yu-Qing Yang, Xiao-Xia Huang and Jian-Hao Tan. Resources and supervision were performed by Wen-Cheng Fang, Cheng Wang, Chao-Peng Wang and Zhen-Tang Zhao. The first draft of the manuscript was written by Yu-Qing Yang and all authors commented on previous versions of the manuscript. All authors read and approved the final manuscript.

References

- Particle Therapy Cooperative Group (PTCOG) Collaboration. <http://www.ptcog.com>
- E.S. Diffenderfer, B.S. Srensen, A. Mazal et al., The current status of preclinical proton FLASH radiation and future directions. *Med. Phys.* **49**, 2039–2054 (2022). <https://doi.org/10.1002/mp.15276>
- A. Mandapaka, A. Ghebremedhin, D. Farley et al., SU-E-J-35: clinical performance evaluation of a phase II proton CT scanner. *Med. Phys.* **41**(6), 162 (2014). <https://doi.org/10.1118/1.4888087>
- B. Schaffner, E. Pedroni, The precision of proton range calculations in proton radiotherapy treatment planning: experimental verification of the relation between CT-HU and proton stopping power. *Phys. Med. Biol.* **43**(6), 1579–1592 (1998). <https://doi.org/10.1088/0031-9155/43/6/016>
- A.M. Cormack, Representation of a function by its line integrals, with some radiological applications. *J. Appl. Phys.* **34**, 2722–2727 (1963). <https://doi.org/10.1063/1.1729798>
- U. Schneider, J. Besserer, P. Pemler et al., First proton radiography of an animal patient. *Med. Phys.* **31**(5), 1046–1051 (2004). <https://doi.org/10.1118/1.1690713>
- X.Y. Chen, R.R. Liu, S. Zhou et al., A novel design of proton computed tomography detected by multiple-layer ionization chamber with strip chambers: a feasibility study with Monte Carlo simulation. *Med. Phys.* **47**, 614–625 (2019). <https://doi.org/10.1002/mp.13909>
- S. Deffet, M. Cohilis, K. Souris et al., openPR—a computational tool for CT conversion assessment with proton radiography. *Med. Phys.* **48**(1), 387–396 (2021). <https://doi.org/10.1002/mp.14571>
- Y.J. Ma, Y. Ren, P. Feng et al., Sinogram denoising via attention residual dense convolutional neural network for low-dose computed tomography. *Nucl. Sci. Tech.* **32**, 41 (2021). <https://doi.org/10.1007/s41365-021-00874-2>
- K. Chen, L.B. Zhang, J.S. Liu et al., Robust restoration of low-dose cerebral perfusion CT images using NCS-Unet. *Nucl. Sci. Tech.* **33**, 30 (2022). <https://doi.org/10.1007/s41365-022-01014-0>
- E. Oponowicz, H. Owen, Superconducting gantry design for proton tomography, in *Proceedings of IPAC2017, Copenhagen, Denmark* (2017), pp. 4795–4797
- W.C. Fang, X.X. Huang, J.H. Tan et al., Proton linac-based therapy facility for ultra-high dose rate (FLASH) treatment. *Nucl. Si. Tech.* **32**, 34 (2021). <https://doi.org/10.1007/s41365-021-00872-4>
- A. Kamal, Passage of charged particles through matter, in *Nuclear Physics*. (Springer, Berlin Heidelberg, 2014), pp. 1–81
- S.N. Penfold, A.B. Rosenfeld, R.W. Schulte et al., A more accurate reconstruction system matrix for quantitative proton computed tomography. *Med. Phys.* **36**(10), 4511–4518 (2009). <https://doi.org/10.1118/1.3218759>
- D.C. Williams, The most likely path of an energetic charged particle through a uniform medium. *Phys. Med. Biol.* **49**, 2899 (2004). <https://doi.org/10.1088/0031-9155/49/13/010>
- R.W. Schulte, S.N. Penfold, J.T. Tafas et al., A maximum likelihood proton path formalism for application in proton computed tomography. *Med. Phys.* **35**, 4849–4856 (2008). <https://doi.org/10.1118/1.2986139>
- R. Schulte, V. Bashkurov, T.F. Li et al., Design of a proton computed tomography system for applications in proton radiation therapy, in *Proceedings of the 2003 IEEE Nuclear Science Symposium. Conference Record (IEEE Cat. No.03CH37515)*, vol. 3 (2013), pp. 1579–1583. <https://doi.org/10.1109/NSSMIC.2003.1352179>
- Y. Zhang, W.C. Fang, X.X. Huang et al., Design, fabrication, and cold test of an S-band high-gradient accelerating structure for compact proton therapy facility. *Nucl. Sci. Tech.* **32**, 38 (2021). <https://doi.org/10.1007/s41365-021-00869-z>
- Y. Zhang, W.C. Fang, X.X. Huang et al., Radio frequency conditioning of an S-band accelerating structure prototype for compact proton therapy facility. *Nucl. Sci. Tech.* **32**, 64 (2021). <https://doi.org/10.1007/s41365-021-00891-1>
- C. Wang, Z.H. Zhu, Z.G. Jiang et al., Design of a 162.5 MHz continuous-wave normal-conducting radiofrequency electron gun. *Nucl. Sci. Tech.* **31**, 110 (2020). <https://doi.org/10.1007/s41365-020-00817-3>
- C. Wang, J.H. Tan, X.X. Huang et al., Design optimization and cold RF test of a 2.6-cell cryogenic RF gun. *Nucl. Sci. Tech.* **32**, 97 (2021). <https://doi.org/10.1007/s41365-021-00925-8>
- H. Paganetti, Range uncertainties in proton therapy and the role of Monte Carlo simulations. *Phys. Med. Biol.* **57**(11), 99–117 (2012). <https://doi.org/10.1088/0031-9155/57/11/r99>
- J.H. Tan, W.C. Fang, Z.T. Zhao et al., Two-mode polarized traveling wave deflecting structure. *Nucl. Sci. Tech.* **26**(4), 040102 (2015). <https://doi.org/10.13538/j.1001-8042/nst.26.040102>
- W.S. Wan, L. Brouwer, S. Caspi et al., Alternating-gradient canted cosine theta superconducting magnets for future compact proton gantries. *Phys. Rev. Accel. Beams* **18**, 103501 (2015). <https://doi.org/10.1103/PhysRevSTAB.18.103501>
- R.F. Hurler, R.W. Schulte, V.A. Bashkurov et al., Water-equivalent path length calibration of a prototype proton CT scanner. *Med. Phys.* **39**(5), 2438–2446 (2012). <https://doi.org/10.1118/1.3700173>
- V. Giacometti, V.A. Bashkurov, P. Piersimoni et al., Software platform for simulation of a prototype proton CT scanner. *Med. Phys.* **44**(3), 1002–1016 (2017). <https://doi.org/10.1002/mp.12107>
- R.C. Gonzalez, R.E. Woods, B.R. Masters, Digital image processing, third edition. *J. Biomed. Opt.* **14**(2), 029901 (2009). <https://doi.org/10.1117/1.3115362>
- W. Yu, I. Zeng, A novel weighted total difference based image reconstruction algorithm for few-view computed tomography. *PLoS ONE* **9**(10), e109345 (2014). <https://doi.org/10.1371/journal.pone.0109345>
- G.A.P. Cirrone, M. Bucciolini, M. Bruzzi et al., Monte Carlo evaluation of the filtered back projection method for image reconstruction in proton computed tomography. *Nucl. Instrum. Methods* **658**(1), 78–83 (2011). <https://doi.org/10.1016/j.nima.2011.05.061>

Springer Nature or its licensor (e.g. a society or other partner) holds exclusive rights to this article under a publishing agreement with the author(s) or other rightsholder(s); author self-archiving of the accepted manuscript version of this article is solely governed by the terms of such publishing agreement and applicable law.